SGS Modeling Based on a Fine Scale Reconstruction Method

By Z. L. Chen AND N. A. Adams†

School of Aeronautics, Northwestern Polytechnical University, Xi'an, 710072, Shaanxi, China
†Lehrstuhl für Aerodynamik und Strömungsmechanik, Technische Universität München, Boltzmannstr. 15, 85748 Garching b., München, Germany

In Large-Eddy Simulation (LES) it's crucial to construct a proper SGS model to reproduce the interactions between the resolved and subgrid scales including energy backscatter. In order to correctly model the energy transfer between resolved and subgrid scales, a fine scale reconstruction subgrid model (FSRM) is proposed based on a second generation wavelet method. The model is based on a hard deconvolution in physical space and a subgrid-scale reconstruction in scale space. The deconvolution is realized by an approximate local deconvolution method (ALDM). The reconstruction is built on the lifting scheme under the assumption of scale similarity. The velocity decomposition and reconstruction method is described and validated on the one, two and three dimensional velocity field in detail. This method can be used to decompose or reconstruct scale by scale in a series of frequency bands. One of the FSRM model is presented and validated on decaying grid turbulence, decaying homogeneous turbulence at $Re \to \infty$ and the transition of Taylor-Green vortex. The results show that the present model can well predict the energy spectra and laminar to turbulent transition, and can improve energy spectra near the grid cut-off wavenumber compared with ALDM model.

1. Introduction

In Large-Eddy Simulation (LES), large-scale structures are directly resolved from the filtered Navier-Stokes equation, while the effects of filtered small-scale structures on resolved scales are modeled by a subgrid-scale (SGS) model. Therefore, it's crucial to construct a proper SGS model to reproduce the interactions between the resolved and subgrid scales.

Most SGS models are based on the classical homogeneous turbulence theory, which cannot correctly simulate energy transfer, e.g., energy backscatter. In the classical turbulence theory, it is supposed that small scales function as dissipation scales. These dissipation scales are dynamically universal and are independent of large energy-production scales. It is also supposed that there are a large range of inertial scales separate the large and small scales. These assumptions are invalid in wall-bounded turbulence, where the small scales approaching Kolmogorov length scale are found dynamically very important. Most of the turbulent kinetic energy is produced by small scales in the buffer layer at moderate Reynolds number and by large scales in the logarithmic layer at high Reynolds number [1], which is much larger than local dissipation. As a result, energy fluxes occur in physical and energy backscatter happens in scale space. In order to simulate the dynamics of the small scale near the wall, the grid should be fine enough to represent the fine scales, which leads to huge computational resources requirements at high Reynolds number and makes LES restricted in moderate Reynolds turbulence simulation [2, 3].

The complex behavior of wall turbulent flows in the compound space of scales and wall-normal distances as a function of the filter lengths bas been analyzed by means of the filtered generalized Kolmogorov equation for filtered velocity fields of turbulent channel flow [4]. When the filter lengths are very small in streamwise and spanwise directions, the small scale energy source is captured by the filtered computed fields. Hence, the role of the sub-grid scales is to drain resolved energy, without nonlinear energy redistribution effects, and the related phenomenology can be reproduced to a good degree with the commonly used linear eddy viscosity models. When filtering at larger scales, the resolved motion does not capture the main mechanisms of the flow which lie in the small scales. Those subgrid scales are in fact responsible for driving the larger coherent motion through a backward energy transfer, and contribute to a significant nonlinear redistribution of resolved energy. Therefore, it is highly required to construct a SGS model that can reproduce this energy backscatter from the subgrid scales to resolved scales when filtering at larger scales at high Reynolds number.

The inherent mechanism of multiscale energy transfer of wall-bounded turbulence requires that the SGS models can predict energy backscatter. In previous investigations, energy backscatter is introduced into LES by stochastic modeling [5], dynamic Smagorinsky model [6], similarity subgrid-scale model and velocity estimate models [7]. Stochastic modeling has been applied to solve geophysical flows [8], however, this method is based on a conditional averaging technique which cannot correctly simulate the nonlinear interactions between the resolved and subgrid scales. The dynamic Smagorinsky models allows negative viscous coefficients, however, in real application the viscous coefficient should be positive by using the whole or local averaging, otherwise, the simulation would diverge due to the local energy accumulation. The similarity subgrid-scale model uses the similarity hypothesis between the resolved and subgrid scales, which can simulate energy backscatter but has no enough dissipation. Therefore, it is usually combined with an eddy viscosity model. The velocity estimate model estimates the subgrid velocity, which can theoretically model energy scatter and backscatter. Using established properties of nonlinear subgrid-scale interactions, Domaradzki derived deterministic backscatter models for large-eddy simulations [9]. In 2012, Anderson and Domaradzki [10] built new backscatter SGS models using energy transfer between different scales on the basis of the scale similarity. The results is better than dynamic Smagorinsky model when compared with the DNS data. However, the model is very sensitive to explicit filter operator.

Subgrid scale reconstruction is based on the nonlinear interactions between large and small scales to approximate the unfiltered velocity. Therefore, the subgrid stresses tensor can be directly obtained. The crucial issue of this method is to approximate the complex nonlinear interaction between the large and small scales, which can be realized by subgrid scale estimation based on the nonlinear terms and by mathematical deconvolution. Domaradzki established a velocity estimate model [11]. Scotti and Meneveau [12] developed a velocity reconstruction method based on fractal interpolation. Stolz and Adams proposed an Approximate Deconvolution Method (ADM) [13]. The majority of reconstruction models approximate the unfiltered velocity in physical space. The interaction of subgrid scales on resolved scales is controlled by extra dissipative term [13] and numerical truncation error [14, 15], which falls to make full use of the nonlinear interaction between subgrid and resolved scales.

The objective of present work is to build a SGS model that can well approximate the interactions between the resolved and subgrid scales. It is expected that this model can mitigate the resolution requirement in wall-bounded turbulence simulation at high Reynolds number. The model is based on an approximate deconvolution in physical space and a subgrid-scale reconstruction in scale space. The deconvolution is realized by the ALDM method [15]. The reconstruction is built on the second generation wavelet method under an assumption of scale similarity. The SGS model is firstly constructed and validated for isotropic turbulence and then is extended to wall-bounded turbulent channel flow simulation.

2. Subgrid Scale Modeling

SGS modeling is based on the separation of a flow variable $\phi(\mathbf{x}, t)$ into a large-scale resolved part $\overline{\phi}(\mathbf{x}, t)$ and a small-scale residual part $\phi^{'}(\mathbf{x}, t)$ by a spatial convolution filter $\mathbf{G}(\mathbf{x})$,

$$\phi(\mathbf{x}, t) = \overline{\phi}(\mathbf{x}, t) + \phi^{'}(\mathbf{x}, t), \tag{2.1}$$

$$\overline{\phi}(\mathbf{x}, t) = \int_{-\infty}^{+\infty} \phi(\boldsymbol{\xi}, t)\mathbf{G}(\mathbf{x} - \boldsymbol{\xi})d^3\boldsymbol{\xi}. \tag{2.2}$$

To obtain the governing equations of the resolved flow quantities, a commutative filter is applied to the Navier-Stokes equations. The following filtered equations can be obtained

$$\frac{\partial \overline{\mathbf{u}}}{\partial t} + \nabla \cdot (\overline{\mathbf{u}\mathbf{u}}) = -\frac{1}{\rho}\nabla \overline{p} + \nu \nabla^2 \overline{\mathbf{u}}, \tag{2.3a}$$

$$\nabla \cdot \overline{\mathbf{u}} = 0. \tag{2.3b}$$

The non-linear term $\overline{\mathbf{u}\mathbf{u}}$ in the momentum equations is not expressed as a function of the resolved velocity $\overline{\mathbf{u}}$, which makes these equations unclosed.

2.1. *Fine Scale Reconstruction Model*

In the present method, the filtering operation is not performed explicitly, but by using a finite-volume discretization as a top-hat filter on the background staggered Cartesian mesh. The filter can be written as

$$\mathbf{G}(\mathbf{x}_{i,j,k}, \mathbf{x}) = \frac{1}{\Delta x_i \Delta y_j \Delta z_k} \begin{cases} 1, & \text{if } (\mathbf{x}_{i,j,k} + \mathbf{x}) \in \mathbf{I}_{i,j,k}, \\ 0, & \text{otherwise}, \end{cases} \tag{2.4}$$

where a computational cell is

$$\mathbf{I}_{i,j,k} = [x_{i-\frac{1}{2}}, x_{i+\frac{1}{2}}] \times [y_{j-\frac{1}{2}}, y_{j+\frac{1}{2}}] \times [z_{k-\frac{1}{2}}, z_{k+\frac{1}{2}}], \tag{2.5}$$

and Δx_i, Δy_j and Δz_k are the widths of the cell in three coordinate directions. This filter returns a cell average of a function

$$\overline{\varphi}(\mathbf{x}_{i,j,k}, t) = \frac{1}{\Delta x_i \Delta y_j \Delta z_k} \iiint\limits_{\mathbf{I}_{i,j,k}} \varphi(\mathbf{x}_{i,j,k} - \mathbf{x}, t)d\mathbf{x}. \tag{2.6}$$

When this filter is applied to the Navier-Stokes equations, the governing equations of the resolved velocity are obtained as

$$\frac{\partial \overline{\mathbf{u}}_{i,j,k}}{\partial t} + \mathbf{G}(\mathbf{x}_{i,j,k}, \mathbf{x}) * (\nabla \cdot \mathbf{F}(\mathbf{u})) - \nu \nabla^2 (\overline{\mathbf{u}}_{i,j,k}) + \nabla \overline{p}_{i,j,k} = \mathbf{0}, \tag{2.7a}$$

$$\nabla \cdot \overline{\mathbf{u}}_{i,j,k} = 0, \tag{2.7b}$$

where $\mathbf{F}(\mathbf{u}) = \mathbf{uu}$ is the convective flux. Since the unfiltered velocity $\mathbf{u}$ is unknown, these equations are not closed. A solution adaptive deconvolution scheme $\widetilde{\mathbf{G}}^{-1}$ is designed to approximate $\mathbf{G}^{-1}$, which results in the approximately deconvolved velocity $\widetilde{\mathbf{u}}_{\mathbf{N}} = \widetilde{\mathbf{G}}^{-1} * \overline{\mathbf{u}}_{\mathbf{N}}$. Then $\widetilde{\mathbf{u}}_{\mathbf{N}}$ is decomposed into a low frequency residual $\widetilde{\mathbf{u}}_{\mathbf{Ns_{-n}}}$ and a series of higher frequency details $(\widetilde{\mathbf{u}}_{\mathbf{Nd_{-j}}}, j = 1 \cdots n)$ by using a second generation wavelet method based on lifting scheme

$$\widetilde{\mathbf{u}}_{\mathbf{N}} = \widetilde{\mathbf{u}}_{\mathbf{Ns_{-n}}} + \widetilde{\mathbf{u}}_{\mathbf{Nd_{-j}}}, j = 1 \cdots n, \tag{2.8}$$

where $\widetilde{\mathbf{u}}_{\mathbf{Ns_{-n}}}$ can preserve the mean of the $\widetilde{\mathbf{u}}_{\mathbf{N}}$, and $\widetilde{\mathbf{u}}_{\mathbf{Nd_{-j}}}$ have zero means.

A series of $(k+1)$ subgrid velocity details $(\widetilde{\mathbf{u}}^{\mathbf{P}}_{\mathbf{Nd_{-j}}}, j = -k \cdots 0)$ can be predicted by the details $(\widetilde{\mathbf{u}}_{\mathbf{Nd_{-j}}}, j = 1 \cdots n)$ at larger scales under the scale similarity assumption. The whole reconstructed velocity can be obtained as

$$\widetilde{\mathbf{u}}^{*}_{\mathbf{N}} = \widetilde{\mathbf{u}}_{\mathbf{N}} + \widetilde{\mathbf{u}}^{\mathbf{P}}_{\mathbf{Nd_{-j}}}, j = -k \cdots 0, \tag{2.9}$$

which hopefully can account for the energy transfer between resolved and the unresolved scales. Finally, the reconstructed velocity can be used directly in convective flux computation. A modified Lax-Fridriches flux function $\widehat{\mathbf{F}}_{\mathbf{N}}$ is adopted to approximate the physical flux function $\mathbf{F}$.

The discretized equations finally can be written as

$$\frac{\partial \overline{\mathbf{u}}_{i,j,k}}{\partial t} + \frac{1}{V_{i,j,k}} \sum_{\partial \mathbf{I}_{i,j,k}} \widehat{\mathbf{F}}_{\mathbf{N}}(\widetilde{\mathbf{u}}^{*}_{\mathbf{N}}) \cdot \mathbf{n} \Delta S - \nu \nabla^2 (\overline{\mathbf{u}}_{i,j,k}) + \nabla \overline{p}_{i,j,k} = \mathbf{0}, \tag{2.10a}$$

$$\nabla \cdot \overline{\mathbf{u}}_{i,j,k} = 0. \tag{2.10b}$$

As the whole velocity field is approximated, no explicit subgrid model is applied. An adaptive local deconvolution method (ALDM) based on a nonlinear deconvolution operator is adopted to obtain the approximately deconvolved velocity $\widetilde{\mathbf{u}}_{\mathbf{N}}$ [15]. A projection method is used to solve the filtered Navier-Stokes equations. A second-order central scheme is used to discretize the diffusive terms. An explicit third order TVD Rulnge-Kutta method is used for time advancement. The pressure Poisson equation can be solved every sub-step of the Runge-Kutta scheme. In the next section, a velocity decomposition and reconstruction method based on a second generate wavelet is detailed.

2.2. *Decomposition and Reconstruction Based on a Second Generation Wavelet*

Turbulent flow consists of self-similar structures with a wide range of length scales. Multiscale decomposition has gained increasing interest in turbulence for analysis, and has proven to be useful for understanding the evolution of eddies and the interaction between turbulent flow structures at different scales.

The classical Fourier spectrum gives the energy distribution of a signal in the frequency domain and is evaluated over the entire time interval, which losses the localization of transient features and spatial information [16] and is limited to periodic boundary problem. Huang et. al [17] proposed an Empirical Mode Decomposition (EMD) method, and introduced a concept of Hilbert spectrum. However, EMD cannot correctly represent the instantaneous frequency of an intrinsic mode function. And the Hilbert spectrum has no direct physical meaning. Meneveau [18] used continuous wavelets transformation to analyse turbulence and turbulent kinetic energy. In recent years, curvelets have found increasing use for scale decomposition investigation [19]. Classical construction of orthogonal or biorthogonal wavelets on the infinite real line is based on the Fourier transform (FT) and is carried out in the frequency domain. This introduces considerable constraints on the implementation of the wavelets for practical flow analysis.

The second generation wavelets constructed by using lifting scheme [20] does not resort to the FT, and hence, the so-derived basis functions are not necessarily translations and dilations of a mother function, which makes it suitable for problems defined in bounded domains, analysis of data on curves or surfaces, weighted approximations, and irregular grids. Additional important benefits are the fast implementation, which is fully in-place calculation, and perfect reconstruction. Therefore, in this investigation, it is used to achieve a hierarchical decomposition of the turbulent velocity field in the scale space. Under the scale similarity assumption, a fine scale reconstruction model is proposed.

2.2.1. *Scale Decomposition*

The lifting scheme is independent of the Fourier transformation and has three steps: split, predict, and update. An original signal $\lambda_{0,k}$ (k is the length of the data and can be even or odd.) can be split into two subsets:

$$(\lambda_{0,2k}, \lambda_{0,2k+1}) = split(\lambda_{0,k}), \tag{2.11}$$

and let $\lambda_{-1,k} = \lambda_{0,2k}$. The wavelet coefficients $\gamma_{-1,k}$ are obtained in the prediction step as:

$$\gamma_{-1,k} = \lambda_{0,2k+1} - P(\lambda_{0,2k}), \tag{2.12}$$

where P is a prediction operator. Finally, scaling coefficients $\lambda_{-1,k}$ are obtained in the update step as:

$$\lambda_{-1,k} = \lambda_{-1,k} + U(\gamma_{-1,k}), \tag{2.13}$$

where U is an update operator. Then repeat this process to get wavelet and scaling coefficients at large spatial scales. If n levels of scale are decomposed and denote the forward second generation wavelets transformation as 'SWT', then the n times forward transformation can be represented as:

$$(\lambda_{-n,k}, \gamma_{-j,k}) = SWT^n(\lambda_{0,k}), (j = 1 \cdots n, k \in Z). \tag{2.14}$$

The scale decomposition is realized by a layered inverse transformation. The low frequency residual s_{-n} having the same signal length in physical space is calculated from the inverse transformation of the scaling coefficients $\lambda_{-n,k}$:

$$s_{-n} = SWT^{-n}(\lambda_{-n,k}). \tag{2.15}$$

And a high frequency detail d_{-j} at level j is obtained by the inverse transformation of the corresponding wavelets coefficients $\gamma_{-j,k}$:

$$d_{-j} = SWT^{-j}(\gamma_{-j,k}), j = 1 \cdots n. \tag{2.16}$$

Finally the original signal can be perfectly reconstructed as:

$$\lambda_{0,k} = s_{-n} + \sum_{j=1}^{n} d_{-j} = SWT^{-n}(\lambda_{-n,k}, \gamma_{-j,k}), j = 1 \cdots n. \tag{2.17}$$

2.2.2. *Fine Scale Reconstruction*

Based on the view of energy cascade and scale similarity hypothesis of homogeneous turbulence, finer wavelet coefficients $\lambda_{-j,k}$ at level j can be expected as a function of scaling and wavelet coefficients at all the coarse levels as:

$$\gamma_{-j,k} = f(\lambda_{-n,k}, \gamma_{-j-1,k}, \cdots, \gamma_{-n,k}), \tag{2.18}$$

where f is an unknown function. In the consideration of localization of fine scales, it is supposed that the predicted wavelet coefficients $\gamma^p_{-j,k}$ by a model are linear function of its neighbour coarse-level coefficients $\gamma_{-j-1,k}$ and $\gamma_{-j-2,k}$. Therefore, a wavelet coefficient at position x_l can be predicted by using its two neighbours γ_{-j-1,x_m} and γ_{-j-1,x_n} as:

$$\gamma^p_{-j,x_l} = \frac{x_n - x_l}{x_n - x_m} * \gamma_{-j-1,x_m} + \frac{x_l - x_m}{x_n - x_m} * \gamma_{-j-1,x_n}, \tag{2.19}$$

where it supposes $x_m < x_l < x_n$. Then the predicted high frequency detail d^p_{-j} can be obtained by the inverse transformation of $\gamma^p_{-j,k}$ as:

$$d^p_{-j} = SWT^{-j}(\gamma^p_{-j,k}), j = 1 \cdots n. \tag{2.20}$$

Using this model, a higher frequency detail $\gamma^p_{0,2k}$ can be predicted and reconstructed from two highest frequency details $\gamma^p_{-1,k}$ and $\gamma^p_{-2,k}$. Therefore, a finer velocity signal $\lambda^p_{1,2k}$ using $\gamma^p_{0,k}$and $\lambda_{0,k}$ can be built. As $\lambda^p_{1,2k}$ is two times of length of $\lambda_{0,k}$, hence, the length of $\lambda_{0,k}$,$\gamma_{-1,k}$ and $\gamma^p_{-2,k}$ should be doubled. Then the finest details $\gamma^p_{0,2k}$ is predicted as:

$$\gamma^p_{0,2k} = f(\gamma_{-1,k}, \gamma_{-2,k}) \tag{2.21}$$

Finally, the finer velocity signal can be obtained as:

$$\lambda^p_{1,2k} = SWT^{-1}(\gamma^p_{0,2k}, \lambda^p_{0,2k}). \tag{2.22}$$

The procedure of scale decomposition and reconstruction is shown in Fig. 1. The required input to the program is an original signal. All the high frequency detail d_{-j}, low frequency residual s_{-n}, predicted high frequency detail d^p_{-j} and the finer velocity signal can be obtained at one time transformation. Multidimensional transformation can be realized by tensor product of the transform in each direction.

3. Validation of Velocity Decomposition and Reconstruction Methods

The velocity decomposition and reconstruction methods introduced in section 2.2 are validated for one, two and three dimensional turbulent velocity fields.

3.1. *Homogeneous turbulence*

An original data is obtained from the measurements of isotropic grid turbulence at Taylor Reynolds number $Re_\lambda = 720$ [21]. The velocity signal is decomposed into n=9 levels, that is, a series of high frequency details $d_{-j}(j = 1 \cdots 9)$ and a low frequency residual s_{-9}, as shown in Fig. 2. Each high frequency detail represents a series of velocity

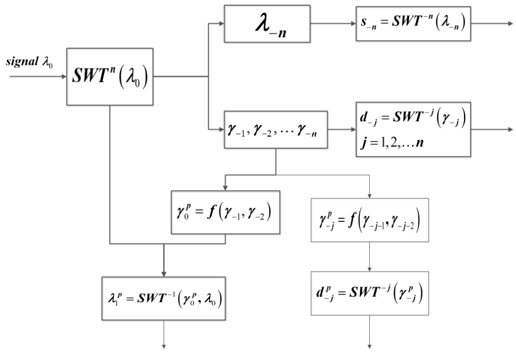

FIGURE 1. Procedure of scale decomposition and reconstruction method.

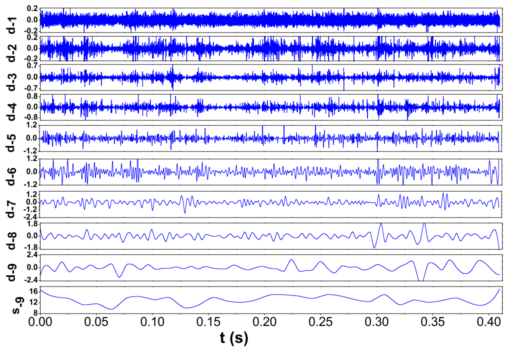

FIGURE 2. Scale velocities obtained at $n = 9$ for homogeneous turbulent velocity at $Re_\lambda = 720$.

at certain scale, which is named scale velocity. The low frequency residual represents the largest scale velocity, which represents the trend of the original signal as shown in Fig. 3. To know the kinetic energy characteristics, FT is done for each scale velocity and original velocity, as shown in Fig. 4. It can be found that each scale-velocity component contributes to the total spectra at its corresponding frequency range. As the scale becomes smaller, the corresponding frequencies become larger and the energy spectra become smaller.

To approach the $-5/3$ Kolmogorov spectrum, one by one Fourier spectrum of $d_{-j}(j = 1 \cdots 9)$ has been adding together to reach low frequency in the inertial range as shown in Fig. 5. It can be seen that the velocity signal is decomposed into three terms: the small scales corresponding to a dissipation range, the large scales corresponding to the energy carrying structures and the moderate scales corresponding to a inertial subrange.

3.2. *Zero-pressure-gradient Boundary Layer*

An original data of a zero-pressure-gradient boundary layer is obtained from the instantaneous velocity fields in a streamwise-wall-normal plane at Reynolds number $Re_\theta = 7705$ ([22]). It contains the streamwise velocity component (u) and the normal turbulent velocity component (v). The fluctuation velocity signals u and v (mean-velocity subtracted) are decomposed into 5 levels. Each scale-velocity component of u and v are combined with coordinate, then correspond vorticity can be calculated from the scale-velocity field. The vorticity contour of scale-velocity is shown in Figure 6. It can be clearly

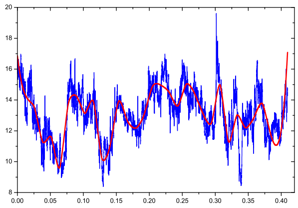

FIGURE 3. Comparison of original velocity and the largest scale velocity component s_{-9}.

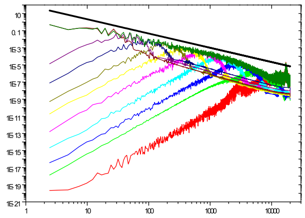

FIGURE 4. Fourier spectrum of d_{-j} $(j = 1 \cdots 9)$. The reference line has slop $-5/3$.

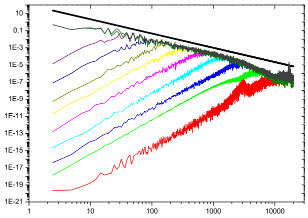

FIGURE 5. Fourier spectrum of the sum of d_{-j} from d_{-1} to d_{-9}, s_{-9}. It shows a clear asymptotic behavior.

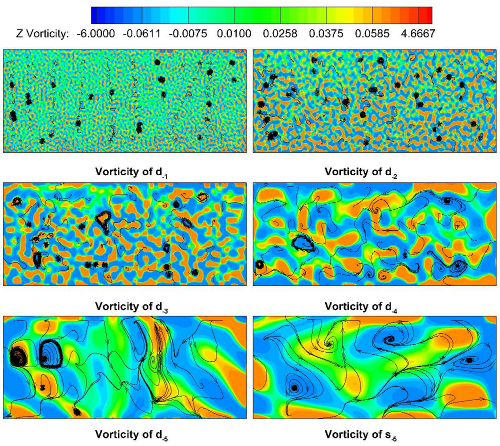

FIGURE 6. Vorticity contour of scale-velocity component.

seen that the the vorticity of scale velocity show a gradual increasing trend from scale velocities d_{-1} to d_{-5}, and the scale of vortex also increases. s_{-5} is the largest scale-velocity, and it contains the largest scale eddy.

The vorticities of scale velocity have been added together and is compared with that the original data as shown in Fig. 7. The difference between them is very small. It can be clearly seen that they are exactly the same and the value of difference is too small, so that it can be ignored. It shows that the vorticity contour also can be reconstituted. The fluctuation velocity signals are decomposed into several scale-velocity corresponding to the vortex has be separated into a set of smaller scale vortex and a bigger scale vortex. Also, the corresponding vorticity can been decomposed.

3.3. *Turbulent Channel Flow*

Nine series of velocity are obtained at nine different wall distances in a DNS of a TCF at $Re_\tau = 206$. The fluctuation velocity signals (mean velocity subtracted) are decomposed into 11 levels. To know the relationship between the largest scale velocities s_{-11} at different wall distances, they are compared in Fig. 8. It can be clearly seen that they have similarity in the buffer and logarithmic regions and that there are time delays from bottom to centre. The correlation coefficients of s_{-11} and original velocity signals at $y^+ = 97.96$ to those at other wall distances are shown in Fig. 9. It is obvious that the correlation coefficients of s_{-11} are much larger than the correlation coefficients of orig-

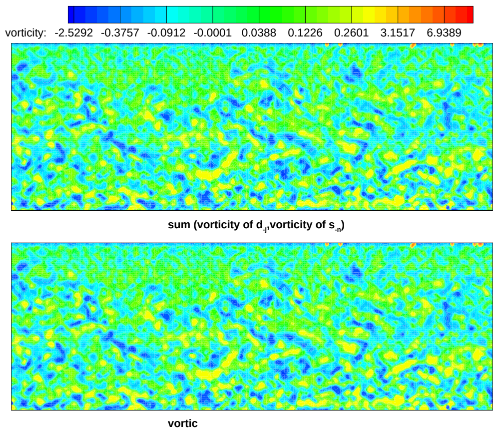

FIGURE 7. Comparison of vorticity for original velocity and summation of scale velocity.

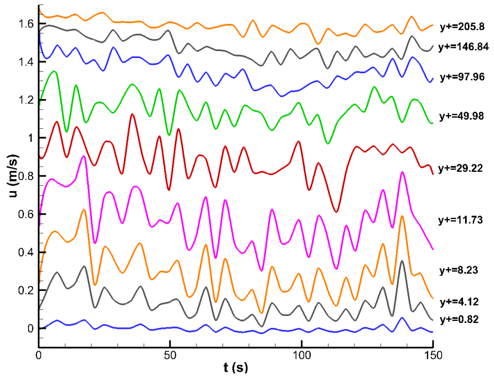

FIGURE 8. Comparison of s_{-11} at different wall distances, each one is shifted 0.2 upwards from $y^+ = 4.12$ for clarity.

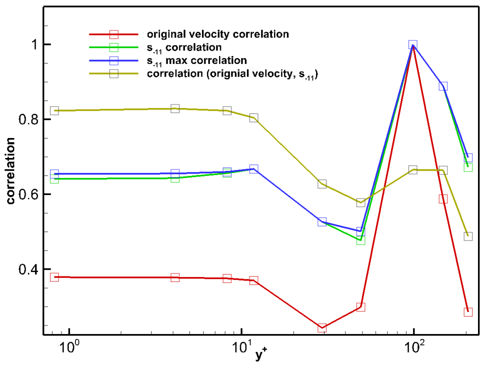

FIGURE 9. Correlation coefficients of s_{-11} and original velocity signals between at $y^+ = 48.98$ and at other y^+.

inal velocity signals. In the consideration of all these large scale velocities are related to a large coherent structure across the half channel, the max correlation coefficients are also computed and presented. All the correlation coefficients increase, except for that at $y^+ = 97.96$ as shown in Fig. 9. The analysis above is consistent with the experimental results of Mathis et al. [23] at high Reynolds number that the large scales in the logarithmic region have modulation effect on the near wall motion.

Four series of instantaneous streamwise velocity in xz plane are obtained at four different wall distances. The velocity signal is decomposed into $n = 5$ levels. From the contour of scale-velocity as shown in Fig. 10, Fig. 11 and Fig. 12, the streak of high and low velocity can be clearly seen. In buffer layer, the streak of high and low velocity has appear in smaller scale velocity like d_{-3}, but the velocity in logarithmic region does not has clear steak. In logarithmic region, the scale velocity d_{-4} begin to appear steak but not clearly, and the scale velocity s_{-5} has show the clear steak.It can be clearly seen that the contour of smaller scale velocity like d_{-3} is similar in the same region but less similar in the different layer. But he contour of larger scale velocity like s_{-5} is similar not only between in same region but also in different layer.

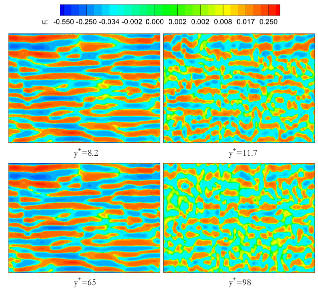

FIGURE 10. Velocity contours of d_{-3} at different wall distances.

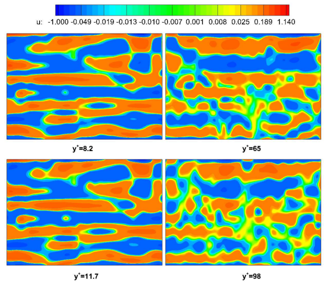

FIGURE 11. Velocity contours of d_{-4} at different wall distances.

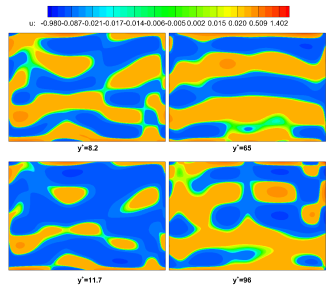

FIGURE 12. Velocity contours of s_{-5} at different wall distances.

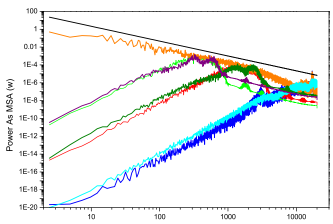

FIGURE 13. Comparisons of Fourier spectrum of reconstructed and original scale velocity. From bottom to top, d^p_{-1}, d^p_{-4}, d^p_{-6}.

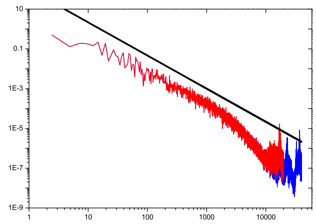

FIGURE 14. Comparison of Fourier spectrum for λ^p_1(blue) and λ_0(red).

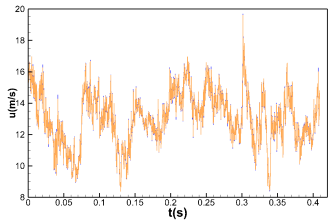

FIGURE 15. Comparison of λ^p_1(blue) and λ_0 (yellow).

3.4. *High Frequency Detail Prediction*

For homogeneous turbulence the finer details can be predicted from its neighbour coarse levels. The details at levels -1, -4 and -6 are reconstructed and their power spectra are compared with the original decomposed scale velocities, as shown in Fig. 13. There are small discrepancies between the predicted and original ones, especially at energy containing frequency.

The original signal can also be extended to finer one using the model in section 2.2.2 without data contamination as shown in Fig. 14 and Fig. 15.

3.5. *Three Dimensional Flow Field Decomposition and Final Scale Prediction*

A three dimensional velocity filed of an arbitrary isotropic homogeneous turbulence produced by LES with resolution $48 \times 48 \times 48$ in a computational domain of $2\pi \times 2\pi \times 2\pi$ cube is used as the original velocity filed. Three levels $n = 3$ of decomposition and two levels $n = 2$ of finer scale prediction are applied. The original velocity can be decomposed into the large scale residual s_{-3} and small scale details $d_{-j}(j = 1, 2, 3)$, as shown in Fig. 16. To validate the accuracy of perfect reconstruction, the decomposed scale velocities are added together and compared with the original velocity, as shown in Fig. 17. It is obvious that the difference between original and reconstructed velocity is trivial. The final scale velocities are predicted at the resolutions 96^3 and 192^3, as shown in Fig. 18. The large scale structures are preserved, and the final scales are predicted from their coarser neighbor details.

From above detailed validations of the velocity decomposition and reconstruction

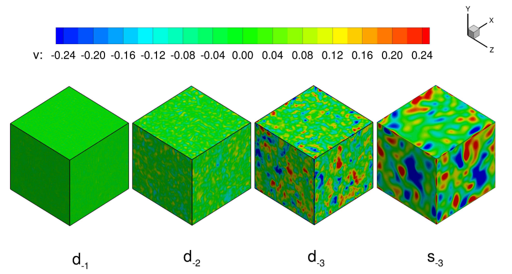

FIGURE 16. Decomposition of 3D velocity with level $n = 3$.Large scale residual s_{-3} and details $d_{-j}(j = 1, 2, 3)$.

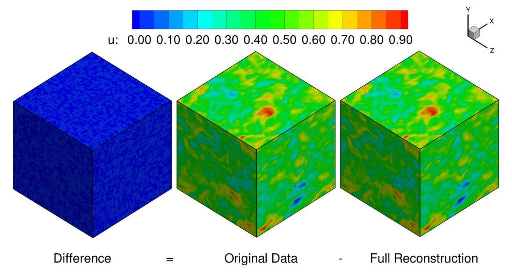

FIGURE 17. Comparison of the 3D original and fully reconstructed velocity.

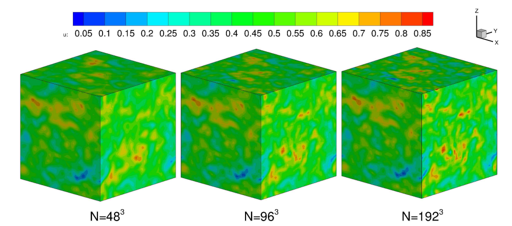

FIGURE 18. Two level finer scale velocity prediction.

method, it can be concluded that it functions correctly for one, two and three dimensional decomposition, reconstruction and prediction, and can be used in the subgrid modeling.

4. A Posteriori Analysis of Fine Scale Reconstruction Model

In LES filtering operator is often nothing but formalism in writing the continuous form of the filtered Navier-Stokes equations. In practice filtering is assumed to be realized by the projective grid filtering, interpolation, discretization and integration schemes. Discretization of a computational domain introduced a characteristic grid length scale. For uniform resolution h, this scale is set by the Nyquist cut-off frequency π/h. If the resolution is nonuniform, the characteristic length cannot easily be ubiquitously defined. It is found that the effective filter length severely depends on the numerical scheme [24]. In the formulation of LES it is assumed that the scales smaller than the Nyquist cut-off associated grid length are completely filtered out. However, in practice there are still lots of small scales between the grid cut-off length and the minimum scales that the gird can

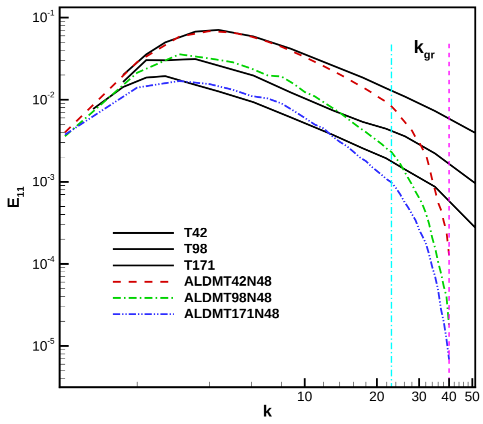

FIGURE 19. Energy spectra of homogeneous turbulence produced with ALDM LES on the resolution 48^3. $k_{cut-off}$ is the wavenumber set by the Nyquist cut-off frequency. k_{grid} is the maximum wavenumber that the grid can support.

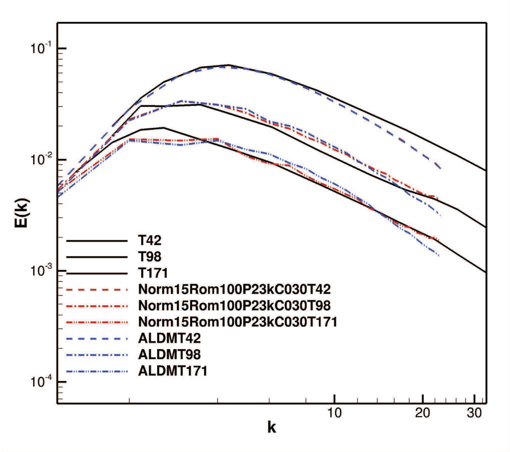

FIGURE 20. Comparisons of energy spectra for the experimental results of Comte-Bellot and Corrsin, LES results of ALDM and FSRM.

support, as shown in Fig. 19. These small scales are partially resolved and are crucial for the energy transfer between the resolved and subgrid scales. It can be seen that the resolved energy spectra at the low wavenumbers near the cut-off wavenumber is under-predicted and has large slope approaching the characteristics of dissipation scales.

In the Fine Scale Reconstruction Model (FSRM) the small scales between the cut-off wavenumber and the maximum grid-supported wavenumber can be manipulated by using the decomposition and reconstruction method. In the investigation these small scales can be isolated, scaled, filtered, reconstructed from its coarser neighbours. A model based the incoherent scales filtering and the fine scale reconstruction can be written as

$$d^*_{-1} = \left\{ \begin{array}{ll} \text{noise}, & |d_{-1}| < C_f |d_{-1}|_{mean} \\ d_{-1}, & |d_{-1}| \geq C_f |d_{-1}|_{mean} \end{array} \right\} + C_p d^p_{-1}, \tag{4.1}$$

in which the modeling coefficients are $C_f = 1.5$, $C_p = 0.3$. d^p_{-1} is predicted from d_{-2} and d_{-3}. In this section only this model is presented on the simulation of decaying grid turbulence, decaying homogenous turbulence at infinity Reynolds number and transition Taylor-Green vortex flow.

4.1. *Decaying Grid-Generated Turbulence*

The computations are initialized with energy spectrum and the Reynolds number is adapted to the wind-tunnel experiments of Comte-Bellot and Corrsin [25]. The flow is modeled as decaying turbulence in a $2\pi^3$-periodic computational box. The energy distribution of the initial velocity field is matched to the first measured energy spectrum. The SGS model is validated by comparing computational and experimental 3D energy spectra at later time instants which correspond to the other two measuring stations, as shown in Fig. 20. It can be seen that with the same initial energy spectrum, the FSRM model can obviously improve the energy spectra near the cut-off frequency compared with the results of ALDM model.

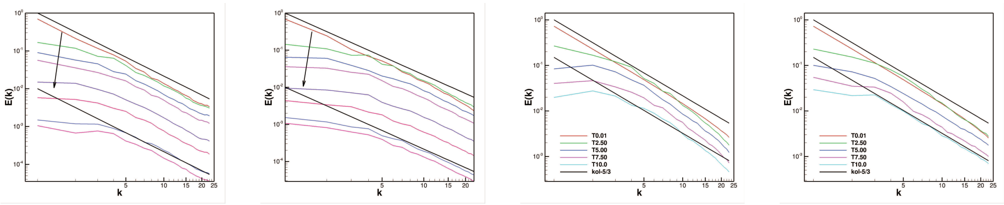

(a) Energy spectra of FRSM model (b) Energy spectra of ALDM model (c) Energy spectra of dynamic Smagorinsky model (d) Energy spectra of WALE model

FIGURE 21. Comparisons of energy spectra for different SGS models in decaying homogeneous turbulence simulation at $Re \to \infty$.

4.2. *Decaying Homogeneous Turbulence at* $Re \to \infty$

The computations are initialized in spectra space with white noise having energy spectrum $k^{-5/3}$. The computational domain is a $2\pi^3$-periodic computational box with resolution 48^3. After an initial transition the energy spectrum decays self-similarly, which can preserves the $k^{-5/3}$ law, as shown in Fig. 21(a). The results of ALDM, dynamic Smagorinsky model and WALE model are also shown in Fig. 21. The ALDM model exhibits weak over-dissipation near the cut-off frequency assembling the results of decaying grid turbulence in the last section. The dynamic Smagorinsky model is too dissipative near the cut-off frequency and cannot preserve the $k^{-5/3}$ scaling law, while WALE model just has slight over-dissipation near cut-off frequency.

4.3. *Transition of the Taylor-Green vortex*

Laminar-turbulent transition is one of the most challenging test case for SGS modeling. The instability modes should be modeled well to predict the onset of transition, neither be stabilized by over-dissipation, nor be early transitioned by under-predicted dissipation. The computational domain is a $2\pi^3$-periodic box with resolution 64^3. The initialization is taken as in the DNS of Brachet et al. [26] at Reynolds number 3000. The energy dissipation rates of FSRM and ALDM are compared in Fig. 22(a). Before time $t = 4$ as there is no small scales developed, the dissipation rate of FSRM is identical as ALDM. Then as there are small scales developed in the wavenumber range from $k_{cut-off}$ to k_{grid}, the FSRM model has large dissipation rate than ALDM. The energy spectra of both models are compared in Fig. 22(b) and Fig. 22(c). FSRM model produces energy spectra having $k^{-5/3}$ scaling law at time $t = 12$, while the results of ALDM also exhibits over dissipation near cut-off frequency at the same simulation time.

5. Conclusions

In order to correctly model the energy transfer between resolved and subgrid scales in large-eddy simulation, a fine scale reconstruction subgrid model (FSRM) is proposed based on a second generation wavelet method. The model is based on an approximate deconvolution in physical space and a subgrid-scale reconstruction in scale space. The deconvolution is realized by the approximate local deconvolution method (ALDM). The reconstruction is built on the lifting scheme under the assumption of scale similarity. First, the resolved velocity is approximately deconvoluted to get approximate velocity. Then approximated deconvolved velocity is decomposed into a hierarchic of scale ve-

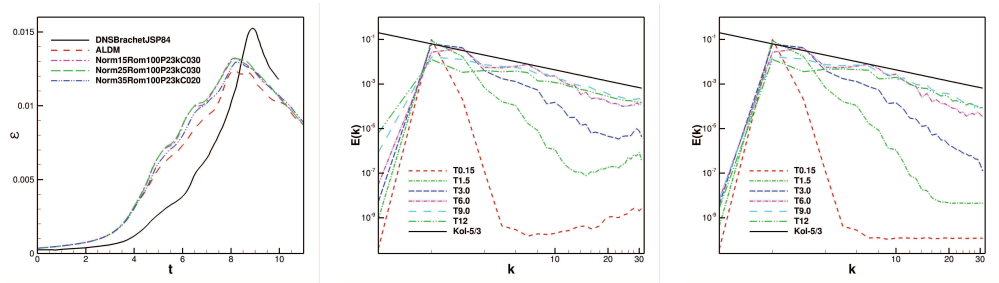

(a) Dissipation rate of FSRM and ALDM (b) Energy spectra of FRSM model (c) Energy spectra of ALDM model

FIGURE 22. Comparisons of dissipation rate and energy spectra for Taylor-Green vortex transition at $Re = 3000$.

locities. The subgrid velocity field is reconstructed by the details of its near bands details. Finally, the whole reconstructed velocity can be used directly in convective flux computation. Therefore, there is no explicit SGS modeling term required.

The velocity decomposition and reconstruction method is described and validated on the one, two and three dimensional velocity field in detail. The results show that the method can be used to decompose or reconstruct scale by scale in a series of frequency bands.

One of the FSRM model is presented and validated on decaying grid turbulence, decaying homogeneous turbulence at infinity Reynolds number and the transition of three-dimensional Taylor-Green vortex. The results show that present model can well predict the energy spectra and laminar to turbulent transition, and can improve energy spectra near the grid cut-off wavenumber compared with ALDM model. This model will be investigated further on wall-bounded turbulence.

Acknowledgments

Financial support has been provided by the German Research Foundation (Deutsche Forschungsgemeinschaft–DFG) in the framework of the Sonderforschungsbereich Transregio 40 and the National Natural Science Foundation of China under the contract No. 11402211. Many thanks to Prof. Dr. J. A. Domaradzki for very helpful discussions.

References

[1] Smits A. J., McKeon B. J., and Marusic I. High-reynolds number wall turbulence. *Annu. Rev. Fluid Mech.*, 43:353–375, 2011.

[2] Hutton. G. The emerging roleof large eddy simulation in industrial practice: challenges and opportunities. *Phil. Trans. R. Soc. A*, 367:2819–2826, 2009.

[3] P. Sagaut. *Large Eddy Simulation for Incompressible Flows: An Introduction*. Cambridge University Press, 2005.

[4] Cimarelli A. and De Angelis E. Anisotropic dynamics and sub-grid energy transfer in wall-turbulence. *Phys. Fluids*, 24:015102, 2012.

[5] Leith C. E. Stochastic backscatter in a subgrid-scale model: plane shear mixing layer. *Phys. Fluids A*, 2:297–299, 1990.

[6] Carati D., Ghosal S., and Moin P. On the representation of backscatter in dynamic localization models. *Phys. Fluids*, 7(3):606–616, 1995.

[7] Domaradzki J. A. and Adams N. A. Direct modelling of subgrid scales of turbulence in large eddy simulation. *Journal of Turbulence*, 3(1)(24), 2002.

[8] Zidikheri M. J. and Frederiksen J. S. Stochastic subgrid-scale modelling for non-equilibrium geophysical flows. *Phil. Trans. R. Soc. A*, 368:145–160, 2010.

[9] Domaradzki J. A. and Saiki E. M. Backscatter models for large-eddy simulations. *Theoretical and Computational Fluid Dynamics*, 9(2):75–83, 1997.

[10] Anderson B. W. and Domaradzki J. A. A subgrid-scale model for large-eddy simulation based on the physics of interscale energy transfer in turbulence. *Phys. Fluids*, 24:065104, 2012.

[11] Domaradzki J. A. and Saiki E. M. A subgrid-scale model based on the estimation of unresolved scales of turbulence. *Phys. Fluids*, 9(7):2148–2164, 1997.

[12] Scotti A. and Meneveau C. A fractal model for large eddy simulation of turbulent flow. *Physica D-Nonlinear Phenomena*, 127(3):198–232, 1999.

[13] Stolz S. and Adams N. A. An approximate deconvolution procedure for large-eddy simulation. *Phys. Fluids*, 11:1699–1701, 1999.

[14] Adams N. A., Hickel S., and Franz S. Implicit subgrid-scale modeling by adaptive deconvolution. *J. Comput. Phys.*, 200:412–431, 2004.

[15] Hickel S., Adams N. A., and Domaradzki J. A. An adaptive local deconvolution method for implicit les. *J. Comput. Phys.*, 213:413–436, 2006.

[16] J.A. Domaradzki and Liu W. An analysis of subgrid-scale interactions in numerically simulated isotropic turbulence. *Phys. Fluids A*, 5(7):1747–1759, 1993.

[17] Huang Y.X. and Schmitt F.G. Analysis of experimental homogeneous turbulence time series by hilbert huang transform. *18eme Congres Francais de Mecanique Grenoble*, pages 27–31, 2007.

[18] Meneveau C. Analysis of turbulence in the orthonormal wavelet representation. *J. Fluid Mech.*, 232:469–520, 1991.

[19] Yang Y. and Pullin D. I. Geometric study of lagrangian and eulerian structures in turbulent channel flow. *J. Fluid Mech.*, 674:67–92, 2011.

[20] Sweldens W. The lifting scheme: A custom-design construction of biorthogonal wavelets. *Appl. Comput. Harmon. Anal.*, 3:186–200, 1996.

[21] Chester S. Kang H. and C. Meneveau. Decaying turbulence in an active-grid-generated flow and comparisons with large-eddy simulation. *J. Fluid Mech.*, 480:129–160, 2003.

[22] R. J. Adrian and Mein H. Vortex organization in the outer region of a turbulent boundary layer. *J. Fluid Mech.*, 422:1–54, 1998.

[23] Hutchins. N Mathis. R and Marusic. I. Large-scale amplitude modulation of the small-scale structures in turbulent boundary layers. *J. Fluid Mech.*, 628:311–337, 2009.

[24] Denaro F. M. What does finite volume-based implicit filtering really resolve in large-eddy simulations? *J. Comput. Phys.*, 230:3849–83, 2011.

[25] Comte-Bellot G. and Corrsin S. Simple eulerian time correlation of full and narrow-band velocity signals in grid-generated 'isotropic' turbulence. *J. Fluid Mech.*, 48:273–337, 1971.

[26] Brachet M. E., Meiron D. I., Orszag S. A., Nickel B. G., Morf R. H., and Frisch U. Small-scale structure of the taylor-green vortex. *J. Fluid Mech.*, 130:411–452, 1983.